Satellite retrieval of cloud condensation nuclei concentrations in marine stratocumulus by using clouds as CCN chambers

Avichay Efraim[1], Daniel Rosenfeld[1], Julia Schmale[2], Yannian Zhu[3]

[1]The Hebrew University of Jerusalem

[2]Paul Scherrer Institute

[3]Meteorological Institute of Shaanxi Province

Key points

- Satellite retrieval of cloud condensation nuclei in shallow marine boundary layer clouds is developed and validated.
- Best validation was achieved for the cores of coupled clouds while accounting for their adiabatic fraction.
- Most of the decoupled clouds had much lower CCN(S) than at the underlying surface indicating mostly surface origination of CCN.

Authors Emails:

Avichay.Efraim@mail.huji.ac.il

Daniel.Rosenfeld@mail.huji.ac.il

Plain text summary

Tiny particles serve as the sites for condensation of cloud droplets, called cloud condensation nuclei. In this study we present a newly developed satellite methodology to quantify these CCN particles which are the basis for creating low-level oceanic clouds. This method was validated against local measurements of particles by vessels in the Southern Oceans, close to Antarctica and in the east mid-Pacific Ocean between California and Hawaii. The results show that this method works best for the brightest clouds that are forming by air that originates at the sea surface. The rest of the clouds are formed on mostly lower drop concentration due to smaller CCN concentrations than at the surface. This indicates that most of the CCN particles are originated from the sea surface and not from above the clouds. This validation of the satellite retrievals allows us to further quantify the relationships between particles in the atmosphere and cloud microphysical properties.

Abstract

A new methodology for satellite retrieval of cloud condensation nuclei (CCN) in shallow marine boundary layer clouds is developed and validated in this study. The methodology is based on retrieving cloud base drop concentrations (N_d) and updrafts (W_b), and calculating the supersaturation (S) based on that. Then N_d is the CCN at S. The accuracy of the satellite retrievals was validated against ship borne measurements of CCN done in recent campaigns in the Southern Oceans (*ACE-SPACE*, *MARCUS* & *PEGASO* [2015-2018]) and in the subtropics (MAGIC [2012-2013]). The satellite retrieve N_d and S at cloud base was related to the actually measured CCN(S) at sea surface. The main findings show that: (a) coupled clouds have good agreement between satellite retrievals and ship measurements of CCN(S); (b) the best agreement is achieved when using the brightest 10% of the clouds, and accounting for their adiabatic fraction, as measured by aircrafts; (c) most of the decoupled clouds had much lower CCN(S) than at the underlying surface. This means that most CCN originate from the surface and not from the free troposphere. This validates the satellite retrievals and allows us to further quantify the relationships between CCN(S) and cloud microphysical properties.

Introduction

Radiative forcing, caused by aerosol-cloud interactions (ACI), has the largest uncertainty and remains the least well-understood anthropogenic contribution to climate change (*IPCC AR5*, 2013). A major cause for this uncertainty is the poorly-quantified aerosols in the pristine pre-industrial atmosphere, such as in the Southern Oceans (SO), which serves as the reference state for anthropogenic cloud radiative forcing. The relatively large N_d of marine stratocumulus (MSC) clouds to the south of 40 °S causes a large cloud cover and reflectance which is underestimated in GCMs (Trenberth and Fasullo, 2010; Naud et al., 2014). According to the GCMs, the SO albedo is lower than it should be. This is important because the region is highly sensitive to cloud cover. Estimating less cloud coverage, induces warm sea surface temperature biases year-round, thus reduces the poleward transport of heat, which increases the error. The ability to retrieve N_d via remote sensing in this vast pristine area, can be used as a proxy for the pre-industrial clouds' situation (Carslaw et al., 2013).

The optical signal of aerosols has been used as proxies for CCN. The most commonly used signal is the aerosol optical depth (AOD) (Feingold et al., 2001; Quaas et al., 2009). An improved proxy is the aerosol index, which is the product of AOD and the Ångström coefficient (Nakajima et al., 2001; Bréon et al., 2002; Lohmann et al., 2002; Gryspeerdt et al., 2017). A recent additional improvement was achieved by using the polarimetric signal of the aerosols to obtain information on their size distribution and concentrations (Hasecamp et al., 2019). However, all these proxies still suffer from uncertainty with respect to matching between the heights of the clouds and of the aerosols that produce the signal. In addition, no aerosol signal is obtained in scenes with nearly full cloud cover. This undermines the possibility to relate cloud large cover to aerosols, while in some situations aerosols are responsible to the transitions between full and broken cloud cover of marine stratocumulus (Rosenfeld et al., 2006; Goren and Rosenfeld, 2012; Goren et al., 2019). The climatological cloud cover of shallow marine boundary layer (MBL) clouds is strongly linked to N_d and starts to decrease strongly at N_d<~80 cm^{-3} (Rosenfeld et al., 2019). Furthermore, at low concentrations aerosols do not produce a useful optical signal for any of the proxies mentioned above. This occurs

at CCN(S=0.4%) <130 cm^{-3} (Shinozuka et al., 2015; Zamora et al., 2016). These concentrations occur at the aerosol-limited regime (Chen et al., 2016), which means that the values of N_d and CCN are close to each other. Most of the ocean areas have Nd<130 cm^{-3} (Grosvenor et al., 2018) which means that the optical aerosol signal is inadequate, even under the most sophisticated processing of its polarimetric signal. Therefore, we have to rely on other methods for quantifying CCN.

Rosenfeld et al. (2016) showed that the CCN can be retrieved from space by using clouds as natural CCN chambers. The N_d is determined by W_b and by the CCN(S), where S is maximum supersaturation. The relationship between S, N_d and W_b is given by:

$$S = C_{(T,P)} W_b^{3/4} N_d^{-0.5} \quad (1)$$

Where C is a temperature and pressure dependent coefficient (Pinsky et al., 2012). In this method, related to convective clouds, N_d is retrieved using a VIIRS-retrieved T−r_e relationship. r_e varies with altitude nearly as in an adiabatic cloud, and therefore adiabatic N_d can be calculated at different altitudes of the cloud using the calculated adiabatic liquid water content (LWC) and r_e. The cloud base N_d is approximated by the adiabatic N_d as calculated by eq. 2 (Freud et., 2011)

$$N_d = \frac{\alpha^3 LWC}{{r_e}^3} \quad (2)$$

$$\alpha = \frac{62.03 r_e}{r_v} \quad (3)$$

where R_v is the cloud drop mean volume radius, as calculated by equally distributing cloud water content between the cloud droplets. The relation between r_e and r_v used here is $r_e = 1.08 r_v$ according to analyzed nonprecipitating clouds by Freud et al., 2011. W_b is calculated by updraft to cloud base height (H_b) relationship found by Zheng et al., (2015):

$$W_b = 0.009 H_b \quad (4)$$

A validation for this method was previously done in the subtropics (fig. 1).

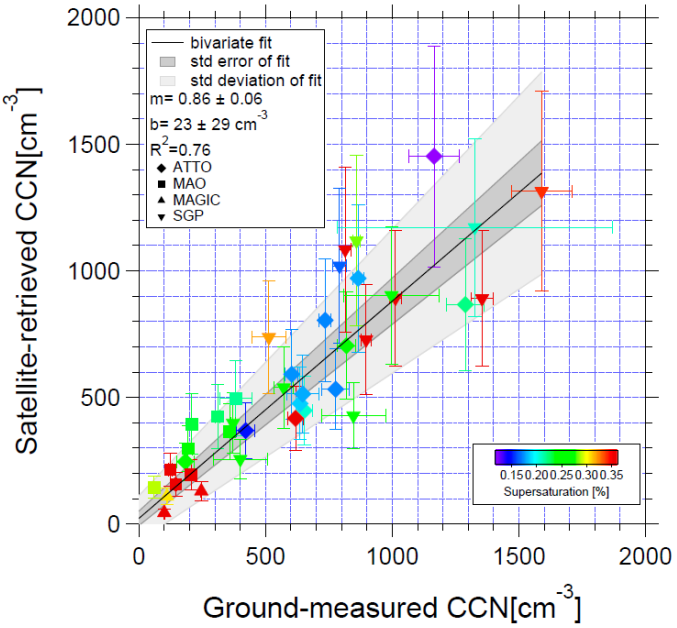

Fig. 1 The relationship between satellite-retrieved CCN at cloud base, and the ground-based instrument measurements of CCN at the same S. The validation data are collected from the DOE/ASR sites on the SGP in Oklahoma and GOAmazon near Manaus, Brazil and over the northeast Pacific (MAGIC). In addition, data are obtained from the ATTO. The location is denoted by the marker shape, and S is shown by the color (Rosenfeld et al., 2016)

MSC clouds are too shallow for satellite retrievals of T-r_e relationships that would be useful for calculating the adiabatic N_d. Therefore, we develop and present here a new methodology for retrieving CCN in MSC clouds. The retrieved CCN are validated against measurements from recent cruise campaigns in the SO (*PEGASO* (2015), *ACE-SPACE* (2016-2017) and *MARCUS* (2017-2018)) and one campaign in the subtropics (MAGIC [2012-2013]) (Table 1 and Fig. 6). The validation is done by relating the satellite retrieved N_d and S to the actual in-situ measured CCN(S) at sea surface.

Methodology

The retrieval of N_d and W_b for MSC clouds is based on a different methodology than the above-mentioned one for convective clouds. The retrieval is based on the Moderate Resolution Imaging Spectroradiometer (MODIS) L2 cloud products on board the Terra and Aqua satellites. We use the r_e and the cloud optical depth ($\boldsymbol{\tau}$) products. Having r_e and τ allows us to calculate the N_d via equation 5:

$$N_d = \frac{\sqrt{5}}{2\pi k}\left(\frac{AF \cdot C_w \cdot \tau}{Q_{ext} \cdot \rho_w \cdot r_e^5}\right)^{\frac{1}{2}} \quad (5)$$

Where C_w is the condensation rate of cloud water in a rising adiabatic cloud parcel [m^{-3} m^{-1}], Q_{ext} is the extinction efficiency factor, which represents the ratio between the extinction and the geometric cross section of a given droplet, approximated to value of 2, ρ_w = 1,000 kg/m3 is the density of liquid water, k relates r_v to r_e ($k = \left(\frac{r_v}{r_e}\right)^3 = 0.8$) and AF is the adiabatic fraction. We initially assume fully adiabatic cloud (AF=1) (Szczodrak et al., 2001; Grosvenor & Woods, 2014; Grosvenor et al., 2018).

N_d is calculated for the brightest 10% of the cloud to get closest to retrieval assumptions of homogeneity and adiabaticity. Taking the top 10% (90th percentile) of the cloud optical depth minimizes bias due to partial pixel filling of clouds and allows focusing on the brightest pixels of the clouds, which are where updrafts are strongest and fed most directly from the air and CCN below cloud base, thus best representing the surface CCN in well mixed boundary layer (fig. 2).

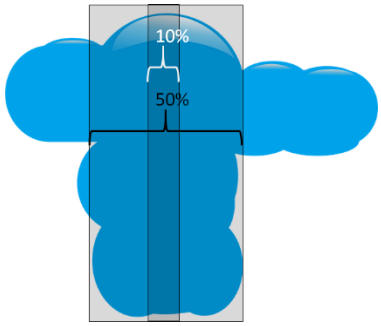

Fig. 2 Cloud selection for retrieved N_d which best representing CCN effects
The brightest part of the cloud, the top 10 percent, is the convective core of the cloud and best represents the full profile of the cloud and the surface CCN.

Zheng et al. (2018) showed that in well-mixed MBLs, W_b is related nearly linearly to cloud top radiative cooling rate (CTRC) (fig. 3). A larger CTRC enhances the entrainment of dry free-tropospheric air, which dries the boundary layer and elevates cloud base height. A lower surface relative humidity increases evaporation, which is manifested in enhanced surface latent heat fluxes. That heat is conveyed towards cloud top to be lost radiatively to space. Therefore, larger heat flux translates to stronger updrafts and higher cloud base.

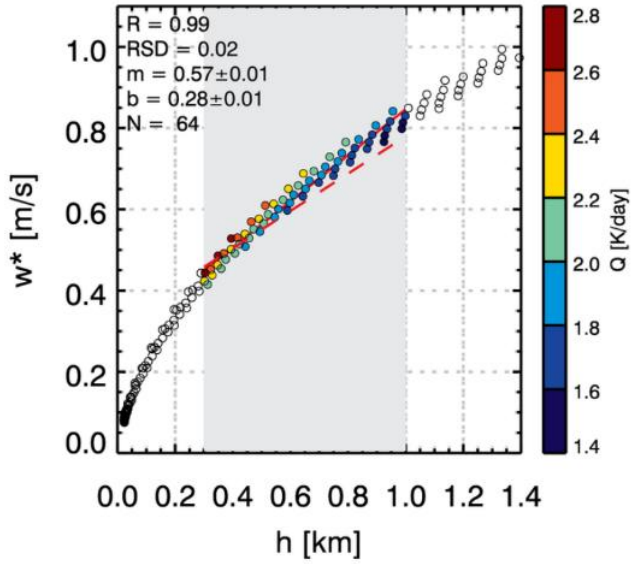

Fig. 3 The scheme of retrieved cloud base updraft.
Q is the radiative cooling rate per unit mass. Dashed red line marks the best-fit line between the observed relationship between cloud base W_b and cloud base height during the MAGIC campaign in Zheng and Rosenfeld (2015).

Cloud base height was retrieved based on the assumption of coupled adiabatic clouds. It was done by using a parcel model, which takes into account different atmospheric profiles according to the cloud's top temperature, liquid water path (LWP) and sea surface temperature (SST) below the cloud, while assuming adiabatic cloud core, and finds the closest atmospheric profile (Goren et al., 2018; Rosenfeld et al., 2019). For a given satellite-retrieved cloud top temperature and LWP there is a unique cloud base height under these assumptions. The implications of deviations from these assumptions are discussed below. In addition, the lifting condensation level (LCL) was calculated based on the vessel-measured surface temperature and dew point. The actual cloud base height over the vessels was measured by a lidar or a ceilometer.

Manually selected polygons containing single layer boundary layer water clouds were selected over or near the vessels measuring CCN below the clouds. The coupling state i.e. whether clouds are feeding on aerosols originating from the surface, was also taken into account. A decoupled cloud is not fed from near-surface air, and therefore the ship borne measurements do not necessarily represent the CCN in the air ingested by the cloud. Decoupling is identified when (1) the difference between the ship-measured LCL and satellite retrieved cloud base height is over 200 meters; (2) when cloud base height measured by the vessel's ceilometer was higher than LCL by more than 200 m; (3) when cloud base temperature difference from satellite and vessel is $\pm 1.8°C$, which is

practically the same as the first condition; (4) when the cloud base height is over 1 km, and (5) when cases are characterized by warm advection. The warm advection was inferred based on SST and wind properties from National Atmospheric Administration (NOAA) and National Centers for Environmental Prediction (NCEP) reanalysis. When an air parcel over higher SST is pushed toward colder SST, it develops a situation where warm air lies above a cooler surface air and thus creates a stable state or a decoupled state, in which the measured air parcels from the vessel and the satellite are not the same.

The CCN counters on the vessels operated cycles of several fixed values of S, producing time series of CCN(S) spectra. The spectra between two hours prior and following a satellite's overpass were used (fig. 4), assuming the same air mass over the vessel for the entire time. To minimize the noise, CCN were taken only for the second half of each new S level, after S has been mostly stabilized.

For a given cloud base N_d, S is smaller for higher temperature due to the increased molecular diffusion rates (Johnson, 1980). The temperature at the center of the CCN counter (around 25±5 °C) is much higher than at cloud base, mainly over the Southern Oceans (-3 °C on average). This requires a correction, where S for cloud base is calculated with Eq. 1 using the CCN temperature instead of cloud base temperature. Additional correction is made by adjusting the cloud base N_d to the surface air density.

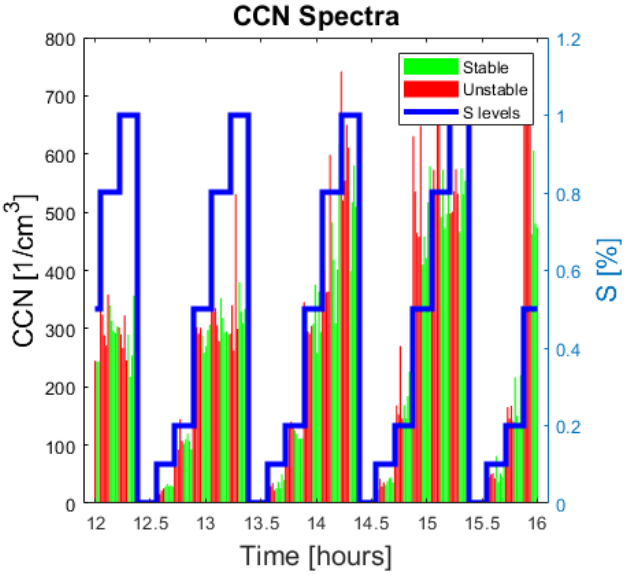

Fig. 4 CCN spectra. The blue line is the S level. The red bars are the CCN measured when the device was not stable. The green bars are the CCN stable measurements that were considered. Out of two hours time, before and after satellite overpass, stable measurements of each S level were used to produce a CCN spectra of the sampled air parcel.

The surface-adjusted satellite retrieved N_d and S are compared to the in situ measured CCN spectra according to the scheme shown in fig. 5, as was first done in Rosenfeld et al. (2014).

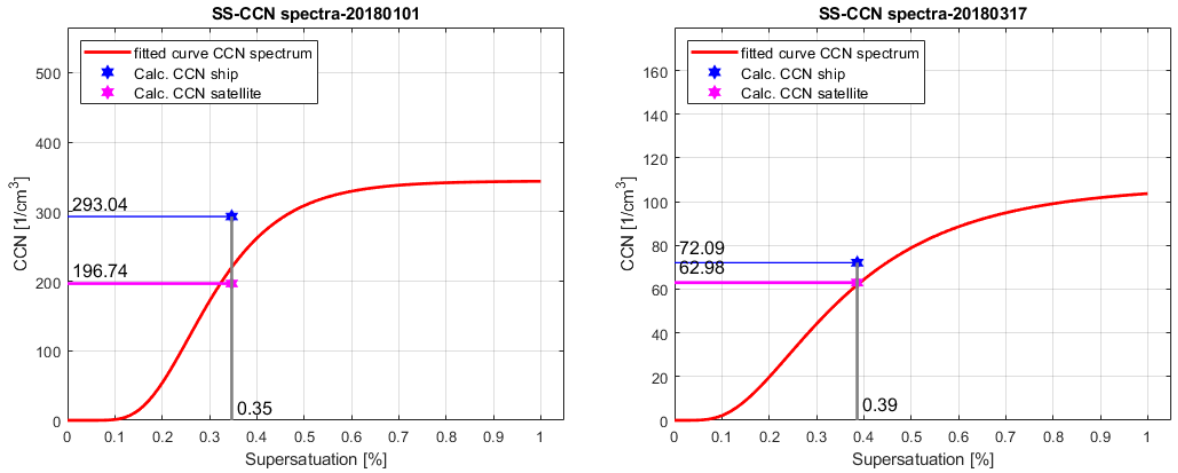

Fig. 5 Retrieved CCN and N_d from vessel and satellite respectively on a CCN spectrum over different S levels. A. A decoupled case where vessel to polygon distance is 79 km. Cloud base height is 445 m. ΔT_b is 7.2°C and ΔH_b is 512 m. B. A coupled case where polygon to vessel distance is 75 km. Cloud base height is 350 m. ΔT_b is 1°C and ΔH_b is 78 m.

Table 1: All research campaigns used in this study:

Campaign	Duration	Course	Platform type	Website
MAGIC	2012/10-2013/09	Los Angeles, CA to Honolulu, HI	Vessel	https://tinyurl.com/r8zxsr2
PEGASO	2015/01-2015/02	Ushuaia, Argentina to Anvers Island via South Georgia Island and South Orkney Islands	Vessel	https://tinyurl.com/soa84t7
ACE-SPACE	2016/12-2017/03	Cape Town, South Africa, through the Indian Ocean to Hobart, Australia, via the Pacific Ocean to Punta Arenas, Chile, and through the Atlantic Ocean back to Cape Town	Vessel	https://tinyurl.com/w6fpbab
MARCUS	2017/10-2018/04	Hobart, Australia to Antarctica	Vessel	https://tinyurl.com/rzvw6xs
SOCRATES	2018/01-02	Hobart, Australia southwards	Aircraft	https://tinyurl.com/r35ayww
CIRPAS	2005-2016	Off the coast of California.	Aircraft	https://tinyurl.com/vvoq2sw

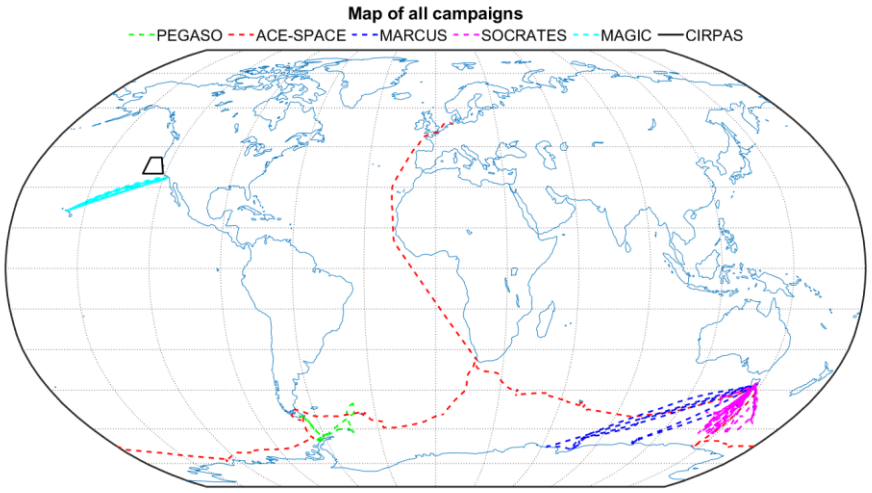

Fig. 6 Map of the courses of the campaigns. The cyan dashed line is the MAGIC campaign course from California to Hawaii. The green dashed line is the PEGASO campaign course from South America to the Antarctic Peninsula. The red dashed line is the ACE-SPACE campaign course around Antarctica and up north. The blue dashed line is the MARCUS campaign course of several legs from Tasmania to Antarctica. The magenta dashed line is the SOCRATES air campaign course of several legs from Tasmania south towards Antarctica. The black line is the CIRPAS air campaign off the coast of California.

Validation & discussion

Out of total of 308 overpasses of the satellites, only 185 cloud scenes were at an acceptable distance (< 150 km) from the vessel to be analyzed. Eventually, 16 cases were found suitable for comparison with the vessel. Cases defined as non-suitable were filtered out by the above-mentioned filtering criteria of coupling state and by being non-shallow clouds with geometric thickness (CGT) of over 800 meters.

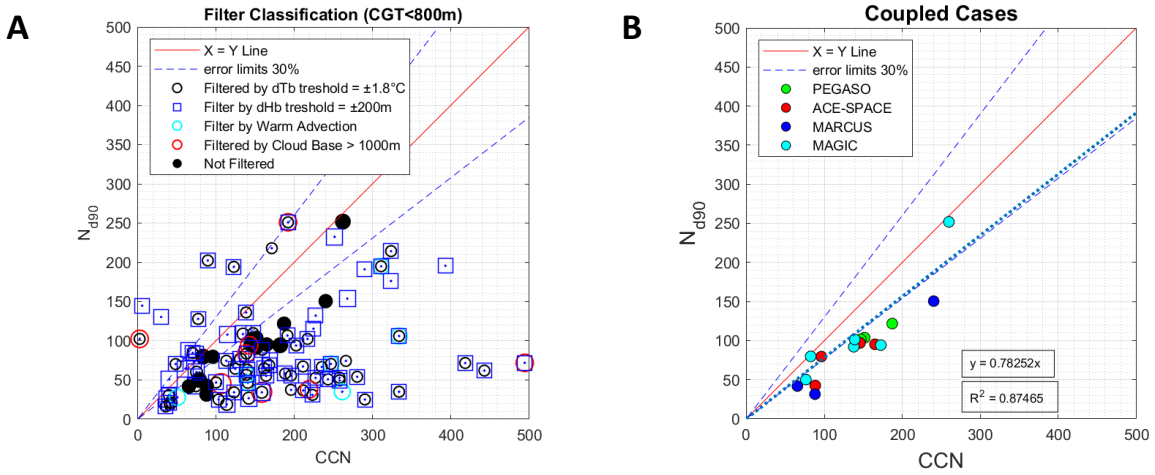

Fig. 7 In panel A are shown all the cases of CGT up to 800 meters marked by their filtering criteria. The black circles are cases filtered out due to $\Delta T_b > 1.8°C$ or $< -1.8°C$. The blue squares are the cases filtered out due to $\Delta H_b > 200\ meters$. The cyan circles are the cases filtered out due to warm advection. The red circles are the cases filtered out due to cloud base height over 1000 meters. The black circles are the coupled cases not filtered by any of the criteria above. In panel B are shown only the coupled unfiltered cases marked by the different validation campaigns: PEGASO (green), ACE-SPACE (red), MARCUS (blue) and MAGIC (cyan). There is an underestimation by a factor of ~ 1.3 of the N_{d90} to the measured CCN concentration from the vessel and $R^2 \approx 0.875$.

As shown in fig 7B, the satellite and in situ measured CCN are well correlated for coupled cases, but there is a systematic underestimation by a factor of 1.278 (slope of correlation is 0.78252) in the retrieved N_d from the satellite with respect to the in situ measured CCN at the cloud base S.

A possible explanation for this underestimation is AF, which represents how close is the cloud to the adiabatic assumption. It is defined as the ratio between the actual LWP profile of a cloud to its adiabatic LWP profile, based on the cloud base and top temperatures and pressures. Taking the 90th percentile in the above results, the clouds are assumed to be fully adiabatic, thus $AF = 1$.

Isolating AF from eq. 5 we get:

$$N_d = \frac{\sqrt{5}}{2\pi k}\left(\frac{C_w \cdot \tau_c}{Q_{ext}\rho_w r_e^5}\right)^{\frac{1}{2}} \cdot \sqrt{\boldsymbol{AF}} \qquad (6)$$

So, N_d is underestimated as a square root of AF:

$$N_{d\,corrected} = \frac{N_{d\,original}}{\sqrt{AF}} \qquad (7)$$

In order to determine the AF from the satellite, we relate the AF to the CGT. The thicker the cloud gets, the lower the AF, because there is more vertical distance for the cloud to mix with ambient air and reduce droplet concentration. Climatology of clouds' CGT was obtained by SOCRATES campaign, using the aircraft's altitude profile, as it flew beneath the cloud, through and above them. Whenever the aircraft measured N_d above a threshold of 5 droplets per cm^3 on an all ascending or all descending leg it was counted as a cloud layer, in which it measured the LWP. The adiabatic LWP was calculated using the aircraft's ambient temperature and pressure at cloud base following eq. 2.34 in R.R. Rodgers' "*A short course in cloud physics*", (1989). Additional data for this climatology was obtained from CIRPAS campaign off the coast of California (Braun et al., 2018). It is shown by the fitting curve the expected behavior of AF as a function of CGT (fig. 8).

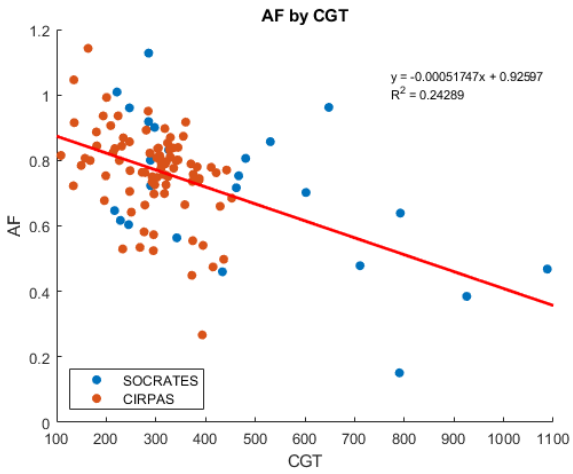

Fig. 8 AF as a function of CGT, as calculated from SOCRATES (blue) and CIPRAS (orange) airborne campaigns. Shown is the expected behavior of decreasing AF as CGT rises, due to larger vertical distance for the cloud to mix with ambient air and reduce droplet concentration.

Applying correction of N_{d90} by AF reduces underestimation by $\sim 7\%$ to a factor of 1.225 (slope is 0.81667) (fig. 9).

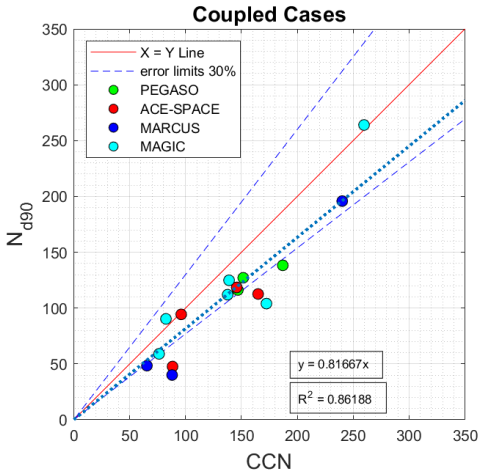

Fig. 9 Coupled cases N_{d90} against CCN after adiabatic fraction correction. Underestimation factor is reduced by 7% to ~1.22 and $R^2 \approx 0.86$

The remaining bias is probably due to (1) systematic decrease of CCN from surface to cloud base with an underestimation factor of up to 1.15; and (2) previously validation for convective clouds that showed uncertainty of $\pm 30\%$ (Rosenfeld et al., 2016).

As shown in figure 12, the results are within the error limits of $\sim 30\%$ and applying the above factors may bring the ratio to unity.

Applying corrections for all cases, coupled and decoupled (fig. 10), it is noticeable that most of the cases (67.4%) fall below the X=Y line and its error limits, meaning that CCN must be originates in the MBL and not in the free troposphere, while only $\sim 16\%$ are above the line, thus originated in the free troposphere.

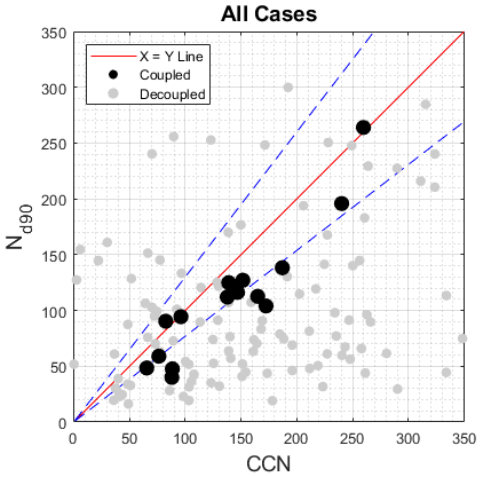

Fig. 10 Coupled and decoupled cases. 67.42% of the cases fall below the lower error limit. 15.91% fall above the upper error limit. 16.67% fall between. The meaning is that most CCN must be originates in the MBL and not in the free troposphere.

Conclusions

Satellite-based assessment of ACI in MBL clouds in now achievable due to validation of satellite retrieval of CCN against in situ measurements, using marine boundary layer clouds as CCN chambers where the N_d and S are retrieved. The retrieved N_d at cloud base is the CCN concentration at the retrieved S and it has been best validated for shallow single layer water MBL coupled clouds.

Two major corrections were performed on the measurements and the retrievals: (1) In order to compare ship-borne S to satellite's S, the temperature difference between the CCN chamber to that at cloud base must be considered, as S increases in lower temperatures, allowing activation of more CCN; (2) Correction by the adiabatic fraction, which assumed to be 1 – a fully adiabatic cloud. Even though the 90^{th} percentile of the sampled cloud is taken (most convective core of the cloud), assuming adiabatic and homogenous cloud, as the cloud thickens, there is more vertical distance for ambient air to mix with the cloud and to negates that assumption. Applying correction by the true adiabatic fraction, obtained by cloud geometrical thickness, reduces bias of N_d to CCN by 7%.

CCN concentrations near the surface of the ocean, in the MBL, are larger than in the cloud base. This gradient of decreasing CCN from surface upward indicates a dominant source from the surface of CCN.

Acknowledge

This research was funded by the Ministry of Science and Technology under Grant 3-13602.

The MODIS data for this study are available and accessible from NASA website. (https://search.earthdata.nasa.gov/search).

The SST and wind reanalysis data are available and accessible from NOAA and NCEP websites. (https://rda.ucar.edu/, https://www.esrl.noaa.gov/)

The MODIS-GUI matlab code was written and developed by Zhu et al. of the Meteorological Institute of Shaanxi Province, Xi'an, China (2018).

References:

Braun, R. A., Dadashazar, H., MacDonald, A. B., Crosbie, E., Jonsson, H. H., Woods, R. K., … Sorooshian, A. (2018). Cloud Adiabaticity and Its Relationship to Marine Stratocumulus Characteristics Over the Northeast Pacific Ocean. *Journal of Geophysical Research: Atmospheres*, *123*(24). https://doi.org/10.1029/2018JD029287

Breon, F.-M. (2002). Aerosol Effect on Cloud Droplet Size Monitored from Satellite. *Science*, *295*(5556), 834–838. https://doi.org/10.1126/science.1066434

Carslaw, K. S., Lee, L. A., Reddington, C. L., Pringle, K. J., Rap, A., Forster, P. M., … Pierce, J. R. (2013). Large contribution of natural aerosols to uncertainty in indirect forcing. *Nature*, *503*(7474), 67–71. https://doi.org/10.1038/nature12674

Chen, J., Liu, Y., Zhang, M., & Peng, Y. (2016). New understanding and quantification of the regime dependence of aerosol-cloud interaction for studying aerosol indirect effects: Aerosol-Cloud Interaction Regimes. *Geophysical Research Letters*, *43*(4), 1780–1787. https://doi.org/10.1002/2016GL067683

Feingold, G., Remer, L. A., Ramaprasad, J., & Kaufman, Y. J. (2001). Analysis of smoke impact on clouds in Brazilian biomass burning regions: An extension of Twomey's approach. *Journal of Geophysical Research: Atmospheres*, *106*(D19), 22907–22922. https://doi.org/10.1029/2001JD000732

Freud, E., Rosenfeld, D., & Kulkarni, J. R. (2011). Resolving both entrainment-mixing and number of activated CCN in deep convective clouds. *Atmospheric Chemistry and Physics*, *11*(24), 12887–12900. https://doi.org/10.5194/acp-11-12887-2011

Goren, T., Kazil, J., Hoffmann, F., Yamaguchi, T., & Feingold, G. (2019). Anthropogenic Air Pollution Delays Marine Stratocumulus Breakup to Open Cells. *Geophysical Research Letters*, 2019GL085412. https://doi.org/10.1029/2019GL085412

Goren, T., & Rosenfeld, D. (2012). Satellite observations of ship emission induced transitions from broken to closed cell marine stratocumulus over large areas: AEROSOLS INDUCE CLOUD REGIME CHANGES. *Journal of Geophysical Research: Atmospheres*, *117*(D17), n/a-n/a. https://doi.org/10.1029/2012JD017981

Goren, T., Rosenfeld, D., Sourdeval, O., & Quaas, J. (2018). Satellite Observations of Precipitating Marine Stratocumulus Show Greater Cloud Fraction for Decoupled Clouds in Comparison to Coupled Clouds. *Geophysical Research Letters*, *45*(10), 5126–5134. https://doi.org/10.1029/2018GL078122

Grosvenor, D. P., & Wood, R. (2014). The effect of solar zenith angle on MODIS cloud optical and microphysical retrievals within marine liquid water clouds. *Atmospheric Chemistry and Physics*, *14*(14), 7291–7321. https://doi.org/10.5194/acp-14-7291-2014

Grosvenor, Daniel P., Sourdeval, O., Zuidema, P., Ackerman, A., Alexandrov, M. D., Bennartz, R., … Quaas, J. (2018). Remote Sensing of Droplet Number Concentration in Warm Clouds: A Review of the Current State of Knowledge and Perspectives. *Reviews of Geophysics*, *56*(2), 409–453. https://doi.org/10.1029/2017RG000593

Gryspeerdt, E., Quaas, J., Ferrachat, S., Gettelman, A., Ghan, S., Lohmann, U., … Zhang, K. (2017). Constraining the instantaneous aerosol influence on cloud albedo. *Proceedings of the National Academy of Sciences*, *114*(19), 4899–4904. https://doi.org/10.1073/pnas.1617765114

Gysel, M., & Stratmann, F. (2013). WP3-NA3: In-situ chemical, physical and optical properties of aerosols. *Deliverable D3*, *11*.

Hasekamp, O. P., Gryspeerdt, E., & Quaas, J. (2019). Analysis of polarimetric satellite measurements suggests stronger cooling due to aerosol-cloud interactions. *Nature Communications*, *10*(1), 5405. https://doi.org/10.1038/s41467-019-13372-2

IPCC, 2013: Summary for Policymakers. In: Climate Change 2013: The Physical Science Basis. Contribution of Working Group I to the Fifth Assessment Report of the Intergovernmental Panel on Climate Change [Stocker, T.F., D. Qin, G.-K. Plattner, M. Tignor, S.K. Allen, J. Boschung, A. Nauels, Y. Xia, V. Bex and P.M. Midgley (eds.)]. Cambridge University Press, Cambridge, United Kingdom and New York, NY, USA.

Johnson, D. B. (1980). The Influence of Cloud-Base Temperature and Pressure on Droplet Concentration. *Journal of the Atmospheric Sciences*, *37*(9), 2079–2085. https://doi.org/10.1175/1520-0469(1980)037<2079:TIOCBT>2.0.CO;2

Lohmann, U., & Lesins, G. (2002). Stronger Constraints on the Anthropogenic Indirect Aerosol Effect. *Science*, *298*(5595), 1012–1015. https://doi.org/10.1126/science.1075405

Nakajima, T., Higurashi, A., Kawamoto, K., & Penner, J. E. (2001). A possible correlation between satellite-derived cloud and aerosol microphysical parameters. *Geophysical Research Letters*, *28*(7), 1171–1174. https://doi.org/10.1029/2000GL012186

Naud, C. M., Booth, J. F., & Del Genio, A. D. (2014). Evaluation of ERA-Interim and MERRA Cloudiness in the Southern Ocean. *Journal of Climate*, *27*(5), 2109–2124. https://doi.org/10.1175/JCLI-D-13-00432.1

Pinsky, M., Khain, A., Mazin, I., & Korolev, A. (2012). Analytical estimation of droplet concentration at cloud base: DROPLET CONCENTRATION AT CLOUD BASE. *Journal of Geophysical Research: Atmospheres*, *117*(D18), n/a-n/a. https://doi.org/10.1029/2012JD017753

Quaas, J., Ming, Y., Menon, S., Takemura, T., Wang, M., Penner, J. E., … Schulz, M. (2009). Aerosol indirect effects – general circulation model intercomparison and evaluation with satellite data. *Atmospheric Chemistry and Physics*, *9*(22), 8697–8717. https://doi.org/10.5194/acp-9-8697-2009

Rogers, R. R., & Yau, M. K. (1996). *A short course in cloud physics* (3. ed., reprint). Oxford: Butterwoth-Heinemann.

Rosenfeld, D., Kaufman, Y. J., & Koren, I. (2006). Switching cloud cover and dynamical regimes from open to closed Benard cells in response to the suppression of precipitation by aerosols. *Atmospheric Chemistry and Physics*, *6*(9), 2503–2511. https://doi.org/10.5194/acp-6-2503-2006

Rosenfeld, Daniel, Fischman, B., Zheng, Y., Goren, T., & Giguzin, D. (2014). Combined satellite and radar retrievals of drop concentration and CCN at convective cloud base: ROSENFELD ET. AL.; RETRIEVING CONVECTIVE CLOUD BASE CCN. *Geophysical Research Letters*, *41*(9), 3259–3265. https://doi.org/10.1002/2014GL059453

Rosenfeld, Daniel, Zheng, Y., Hashimshoni, E., Pöhlker, M. L., Jefferson, A., Pöhlker, C., … Andreae, M. O. (2016). Satellite retrieval of cloud condensation nuclei concentrations by using clouds as CCN chambers. *Proceedings of the National Academy of Sciences*, *113*(21), 5828–5834. https://doi.org/10.1073/pnas.1514044113

Rosenfeld, Daniel, Zhu, Y., Wang, M., Zheng, Y., Goren, T., & Yu, S. (2019). Aerosol-driven droplet concentrations dominate coverage and water of oceanic low-level clouds. *Science*, *363*(6427), eaav0566. https://doi.org/10.1126/science.aav0566

Shinozuka, Y., Clarke, A. D., Nenes, A., Jefferson, A., Wood, R., McNaughton, C. S., … Yoon, Y. J. (2015). The relationship between cloud condensation nuclei (CCN) concentration and light extinction of dried particles: Indications of underlying aerosol processes and implications for satellite-based CCN

estimates. *Atmospheric Chemistry and Physics*, *15*(13), 7585–7604. https://doi.org/10.5194/acp-15-7585-2015

Szczodrak, M., Austin, P. H., & Krummel, P. B. (2001). Variability of Optical Depth and Effective Radius in Marine Stratocumulus Clouds. *Journal of the Atmospheric Sciences*, *58*(19), 2912–2926. https://doi.org/10.1175/1520-0469(2001)058<2912:VOODAE>2.0.CO;2

Trenberth, K. E., & Fasullo, J. T. (2010). Simulation of Present-Day and Twenty-First-Century Energy Budgets of the Southern Oceans. *Journal of Climate*, *23*(2), 440–454. https://doi.org/10.1175/2009JCLI3152.1

Williams, E. (2002). Contrasting convective regimes over the Amazon: Implications for cloud electrification. *Journal of Geophysical Research*, *107*(D20), 8082. https://doi.org/10.1029/2001JD000380

Zamora, L. M., Kahn, R. A., Eckhardt, S., McComiskey, A., Sawamura, P., Moore, R., & Stohl, A. (2016). *Arctic aerosol net indirect effects on thin, mid-altitude, liquid-bearing clouds* [Preprint]. https://doi.org/10.5194/acp-2016-1037

Zheng, Y., Rosenfeld, D., & Li, Z. (2018). The Relationships Between Cloud Top Radiative Cooling Rates, Surface Latent Heat Fluxes, and Cloud-Base Heights in Marine Stratocumulus. *Journal of Geophysical Research: Atmospheres*, *123*(20), 11,678-11,690. https://doi.org/10.1029/2018JD028579